On the Synthesis and Performance of Hierarchical Nanoporous TS-1 Catalysts

Abdul-Lateef Adedigba[a$], Gopinathan Sankar[a]*, C. Richard A. Catlow[a], Yonghua Du[b], Shibo Xi[b], Armando Borgna[b]

[a]*Department of chemistry, University College London, 20 Gordon Street, London WC1H 0AJ, UK*

[$]*Current address: Cardiff Catalysis Institute, Cardiff University, Main building, Park place, Cardiff, CF10 3AT, UK*

[b]*Institute of Chemical and Engineering Sciences, Agency for Science, Technology and Research in Singapore (A*STAR), 1 Pesek Road, Jurong Island, Singapore 627833.*

[*]*Corresponding Author: g.sankar@ucl.ac.uk*

Abstract

Hierarchical TS-1 zeolite was successfully prepared using chitosan as a sacrificial template. The X-ray diffraction showed that the presence of chitosan with the synthesis precursor had no deleterious effect on the crystallinity and phase purity of this zeolite. X-ray absorption spectroscopy at the Ti K-edge, FTIR and Raman spectroscopies revealed the titanium ions in the zeolite structure have predominantly tetrahedral coordination. However, it appears that the higher chitosan content in the synthesis gel imparted some hydrophilic character to the TS-1 system. Furthermore, the technique adopted for the preparation of the synthesis gel – e.g partially dried or fully dried – appears to affect the amount of framework titanium in the zeolite

structure. The calcined form of the chitosan templated TS-1 zeolites exhibited higher cyclohexene conversion compared to the TS-1 material synthesised without this template, but these catalysts showed lower selectivity for cyclohexene epoxide.

KEYWORDS: Hierarchical TS-1, Chitosan, Cyclohexene epoxidation, hydrogen peroxide, XANES, hydrophobic, hydrophilic

1 Introduction

The discovery of titanosilicate molecular sieves opened up a new chapter in the selective oxidation of several substrates under mild conditions of aqueous hydrogen peroxide as an oxidant [1-3]. However, the intrinsic pore geometry of this molecular sieve limits the range of substrates for which it can be used [4], which has led to increased efforts to find ways around this restriction. To overcome diffusion limitations and to facilitate easy access to the active sites of these molecular sieves, several authors have used titanium based large pore molecular sieves [4-7], while others have attempted to create larger pores in the original TS-1 molecular sieve [8-12]; this latter type of material is known as a hierarchical-pore molecular sieve.

Molecular sieves with a hierarchy of pore architectures offer several advantages over those with a predominantly microporous pore structure. Some of these benefits include prolonged activity due to reduced pore blocking, effective diffusion of substrate and products into and from the molecular sieve pore, as well as the ability to accommodate and process bulky molecules that may be larger than the intrinsic zeolite micropore.

There has been intense effort to optimise the synthesis routes to produce molecular sieves with a hierarchy of pores. Commonly employed methods include the use of a secondary (inert) template which can be easily removed by post synthesis thermal treatment in air/oxygen or via chemical treatment [13]. In this category, carbon-based materials such as carbon black (CB) [14, 15], carbon nanotube (CNT) and carbon nanofibre (CNF) [16-19] are popular candidates. However, due to the toxic nature of CB [20] and the high cost of CNT and CNF, alternative materials, which are less toxic and cost effective will be advantageous.

Chitosan, a non-toxic co-polymer derived from deacetylation of chitin is a potential alternative yet to be explored to create hierarchical porous materials. The use of chitosan as sacrificial template offers many advantages as an alternative to carbon black, CNT and CNF as it is widely available at low cost and is non-toxic. Pharmaceutical, food [21, 22], medical [23] and textile [24-26] are some of the industries where chitosan is being used for varieties of applications. In catalysis, however, earlier applications of chitosan include its use for enzyme immobilization and as support for precious and transition metals [27-30].

Although, there are reports on chitosan-zeolite composite systems [31, 32], to the best of our knowledge there are no reports on the application of chitosan as a secondary inert template to develop hierarchical zeolites. Hence, in this study, we report on the direct use of chitosan as a secondary template in the one-pot synthesis of hierarchical TS-1 molecular sieve. The study focuses on the effect of the extent of pre-drying (fully dried or partially dried) of the zeolite precursor on the crystallinity and incorporation of titanium ions in the framework through detailed characterisation of

the chitosan templated TS-1. Titanium K-edge XAS, Raman and infrared spectroscopic techniques were used to determine the incorporation (or otherwise) of Ti^{4+} ions in the framework when synthesised in the presence of chitosan. The catalytic performance of the resulting materials – after calcination – was evaluated for the epoxidation of cyclohexene with aqueous hydrogen peroxide.

2 Materials and Experimental Section

2.1 Materials

All the chemicals utilized in this experiment were sourced commercially. Tetraethyl orthosilicate (TEOS, Research Grade, 98%) and titanium(IV) ethoxide (TEOT, Technical Grade) used as the silica and titanium sources respectively were obtained from Sigma-Aldrich. Tetrapropyl ammonium hydroxide (TPAOH, 25wt% in H_2O) purchased from Acros Organics was used as the structure directing agent. Chitosan (coarse ground flakes and powder, molecular weight 310000 - 375000), used as an inert template was obtained from Sigma-Aldrich. All the chemicals were used as received without further purification or modifications.

2.2 Catalyst synthesis

The TS-1 samples were synthesised hydrothermally. However, the synthesis precursors were prepared in two different ways and the effects of these methods on the structure and activities of the catalysts were investigated.

In the first technique, termed the fully dried method (FD), the precursor was heated to evaporate all the solvent until a dry amorphous powder was obtained. This technique was envisaged to maximize the contact between the zeolite precursor and

the chitosan to induce better mesopore on the resulting zeolite; it also minimises the phase separation between the zeolite precursor and the chitosan. In the second technique, the partially dried method (PD), the precursor was heated for a limited time. This technique, which is closely similar to the conventional hydrothermal method was designed in order to ascertain the effect of the preparation conditions and precursor water content on the zeolite structure. The typical synthesis procedure for both methods is described below.

2.2.1 FD Technique

Typically, 0.5g TEOT was slowly added to 22.85g of TEOS under vigorous stirring at room temperature for an hour. To this solution, 4.45g of TPAOH (25wt% in H_2O) was added dropwise over a period of 15-20 minutes. The resulting mixture was stirred for another one hour, after which the beaker containing the mixture was suspended in an oil bath placed on a magnetic hotplate stirrer and heated to 45^OC with continuous stirring for two hours. After this, a specified amount of chitosan was added to the mixture and stirred at 45^OC for an additional three hours. Subsequently, the temperature of the oil bath was increased to 80^OC and the precursor was left overnight (ca 16 hours) to obtain a dry powder.

The dry powder was mixed with 10.6g of 25wt% TPAOH/H_2O resulting in a viscous mixture with overall average gel composition of 50Si : Ti : 8.5TPAOH : 204H_2O, was charged into a Teflon-lined autoclave, sealed and placed in an oven at 170^OC for 48 hours. After this, the autoclave was quenched in cold water and the solid product retrieved by centrifugation at 4000 rpm. The product was washed several times with deionised water until the pH of the filtrate was below 7.5. The recovered product was

dried overnight at 110^{O}C in an oven. The occluded template molecules (both chitosan and TPAOH), were removed by calcination in static air at 650^{O}C for 12 hours.

2.2.2 PD Technique

This method follows that described for the FD method above until the chitosan was added. Once the chitosan has been added, the mixture was heated at 80^{O}C only for three hours rather than to dryness as in the FD method. Subsequently, 10.6g of TPAOH was then added and the mixture was placed in a Teflon-lined autoclave and crystallized following the conditions described for the FD above. The post synthesis treatment of this samples – separation, washing and calcination – also follow those described for the FD method.

2.3 Characterisation Techniques

The phase purity and crystallinity of the synthesized materials were evaluated using the XRD technique. Diffraction data were recorded from 5-50^{O} 2θ angle using a Bruckner D4 Endeavor X-ray diffractometer with Cu-Kα Radiation (operated at 40KV and 50mA) and a nickel filter.

Raman spectroscopy and X-Ray absorption spectroscopy (XAS) were used to obtain information on the incorporation and coordination geometry of the titanium in the TS-1 structure. In particular titanium K-edge XANES data were used to extract the coordination environment around the titanium in the samples. The Raman spectra were recorded on a multiline Renishaw Invia Raman microscope using a laser wavelength of 325nm. The spectral resolution was set at 4 cm^{-1} and an average of 30 scans was accumulated per sample.

The titanium K-edge XANES data were collected at the XAFCA [33] beam line at the Singapore Synchrotron Light Source (SSLS), Singapore, which operates at 0.7 GeV. In a typical XANES experiment, pellets of the samples were loaded into the *in-situ* cell and heated in vacuum to 773K and the data were recorded during the heating process to evaluate any structural changes in the samples during the removal of adsorbed water. A typical scan time of about 20 minutes per scan was used. The XANES data were recorded in the fluorescence mode using a Bruker detector. $Ti(OSiPh_3)_4$ and ETS-10 were used as standards in the XANES experiment to evaluate the coordination environment of the titanium centres in the samples following the procedure detailed elsewhere [34].

FTIR analysis was conducted using a Bruker Alpha FTIR spectrometer. An average of 16 scans was accumulated for every sample. Morphological characteristics of the samples were obtained using a JOEL field emission-Scanning electron microscope (JSM-6301F) operated at an accelerated voltage of 5kV. Prior to imaging, a finely-ground powder of each sample was sprinkled on the SEM stub and coated with Au using a sputter coater, which was done to enable charge dissipation through the samples.

Elemental analysis was conducted on a Hitachi tabletop microscope TM3030Plus. Powder of each sample was firmly pressed on one side a double-sided carbon tape to achieve a smooth surface. The other side of the carbon tape was affixed to the sample stub.

2.4 Catalytic Testing

The catalytic activity of the calcined samples was evaluated for alkene epoxidation. Cyclohexene was chosen as the model feed and the reaction was conducted in a 50 mL round bottom flask fitted with a reflux condenser. Typically, 6 mmol of cyclohexene, 6 mmol of H_2O_2 (30 wt% in H_2O), 10 mL acetonitrile (solvent) and 0.5 mL mesitylene (used as internal standard) were charged into the reactor. The reaction mixture was thoroughly stirred at room temperature before 100 mg of the catalyst was charged into the reaction vessel. The set-up was heated in an oil bath maintained at 333K and the reaction was carried out for 6 hours under vigorous magnetic stirring. The products of the reaction were analysed using a gas chromatograph (Perkin Elmer Clarus 500) equipped with flame ionization detector (FID) and an Elite-1 capillary column with dimensions of 30m*0.32mm*3µm.

3 Results and Discussions

We investigated TS-1 samples prepared by three different methods: (a) TS-1 produced by conventional methods, (b) TS-1 produced by using fully dried gel and (c) TS-1 from partially dried gel. The reason being that, it is our aim to evaluate the consequence of drying the gel on the phase purity, porosity, hydrophilic/hydrophobic character of the material and more importantly the incorporation of titanium in the framework. Here, we discuss first the characterisation of the samples by a variety of techniques, followed by the results of the catalytic testing.

3.1 Characterisations

3.1.1 Structural Analysis of the Samples

The powder diffraction patterns of all the synthesized samples were compared to that of a reference TS-1 sample synthesized without chitosan. The diffraction pattern of the samples synthesised with chitosan using both techniques match well with that of the reference sample (see figure 1). There were no extra peaks detected in the diffraction patterns, which clearly shows that the presence of chitosan in the synthesis gels had no inhibiting effect on the formation of a good crystalline, phase pure TS-1 samples with the MFI structure.

3.1.2 Morphological Characterisation

The scanning electron micrographs of these samples are presented in figure 2. The images show surface roughness at varying degrees with increasing concentrations of chitosan in the synthesis medium. This roughness can be taken as an indication of extra porosity in the zeolite samples as previously reported by several authors [17, 35-39]. As found for carbon templated zeolites, the zeolites nucleate and grow around the chitosan template [40, 41] and upon calcination, the voids left by the chitosan particles may be responsible for the surface roughness. The TS-1 particle sizes were also estimated from the SEM micrographs and were observed to reduce in size as the chitosan content in the synthesis gel was increased. On taking an average of 30 measured particles, the sizes decreased from 250 nm for the reference sample to 150 nm for the samples synthesised with 10% chitosan. In addition, the samples synthesised with chitosan through the FD method show a very uniformly distributed

particle size, which can be attributed to the principle of “the confined space growth” previously reported with carbon templated growth of ZSM-5 [40, 41].

3.1.3 Spectroscopic Analysis

The FTIR spectra presented in figure 3 show the characteristic MFI absorption bands – at 450, 550, 801, 1100 and 1220 cm^{-1}, which can be ascribed to the bend, symmetry and asymmetry stretch of Si-O bond [12] – for all the samples. In addition to these characteristic MFI absorption bands, a strong absorption band at 960 cm^{-1}, which is characteristic of the Si-O-Ti stretching vibration [42] in the titanium containing samples can be observed. The presence and strength of this peak are the first indications of the existence of the titanium atoms in the tetrahedral framework position, particularly when compared to the spectra of the pure silicate material, which is devoid of this band.

The presence of Raman bands at 960 and 1125 cm^{-1} is generally accepted as evidence of the presence of the titanium species in tetrahedral coordination [43-46]. As shown in figure 4, all the samples – with and without chitosan in the starting synthesis gel – clearly display strong peaks at both 960 and 1125 cm^{-1}. This observation further demonstrates that chitosan in the synthesis precursor plays no inhibiting role in the insertion of the titanium in the TS-1 framework and in the tetrahedral state.

Ti K-edge XAS measurements, performed on all the synthesized samples further corroborate the above findings. The pre-edge features of the synthesized samples were compared with those of two model compounds containing titanium in known coordination states – tetrahedral and octahedral – as shown in figure 5. All the samples synthesized with and without chitosan show pre-edge peak features similar to

that of the model compound $Ti(OSiPh_3)_4$, whose titanium atoms are present in tetrahedral coordination [47]; the other model system, ETS-10 has its titanium atoms in six coordinated state [34, 48] and display lower pre-edge intensity. The presence of chitosan in the synthesis precursor, however, exerts some influence on the pre-edge intensity of the samples. For example, and as presented in table 1, the samples synthesised with chitosan display slightly lesser pre-edge intensity compared to those synthesised in the absence of chitosan. In addition, the degree of loss of the pre-edge intensity was proportional to the amount of chitosan in the starting synthesis precursor. Consequently, the samples with 10% chitosan showed the lowest pre-edge peak intensity.

Nonetheless, the position of the pre-edge of the synthesised samples remained close to that of the model compound, $Ti(OSiPh_3)_4$ in which titanium ions are in tetrahedral coordination [47], implying that the titanium in the synthesised zeolites are largely present in the tetrahedral state.

From table 1, it is clear that the pre-edge intensities of the hydrated samples obtained through the PD method are higher than those obtained via the FD procedure. Such observation may be attributed to different factors. First, it is known that titanium K-edge pre-edge peak intensity is inversely proportional to the coordination state of the titanium in the framework [2], hence, the reduced pre-edge intensity observed for the FD samples – and for all samples synthesised with chitosan – could imply that some higher coordinated titanium species such anatase and rutile are present in these samples, which would possibly imply that the FD samples have lesser titanium atoms in the framework position compared to the PD samples. Coordination expansion around

some of the titanium sites in the FD samples through interaction with water molecules [34, 48, 49] is another likely reason for the lower pre-edge intensities observed for these sets of sample.

To probe the first possibility i.e the presence of non-framework titanium species, these samples were investigated further using UV-Vis spectroscopy, which is known to be effective for the detection of TiO_2 [45, 50-53]. The result of this analysis (figure 6) shows evidence of some extra-framework titanium species in the FD samples (particularly the sample synthesised with 10% chitosan) as shown from the tailing of the absorption bands up to 350 nm, which is not observed in the samples from the PD method. This observation implies that the lower pre-edge peak intensity displayed by these samples could be due to the presence of TiO_2 species. Since the pre-edge peak intensity of the PD samples is higher than those of the FD (table 1), – even for the reference samples – it may be postulated that the TiO_2 species originated from the synthesis procedure rather than from the presence of chitosan in the synthesis medium. Therefore, it may be concluded that the PD technique is more efficient in incorporating the titanium into the zeolite framework compared to the FD technique.

To ascertain the possible role of water coordination – hydrophilic sites associated with titanium centres – in the observed decrease in pre-edge intensity when chitosan was used as a macro-templating agent, *in situ* XAS analysis was conducted by dehydrating the catalysts in vacuo. The comparison of the pre-edge peak intensity of each sample before and after dehydration in vacuo – given in figure 7 and 8 and table 1 suggests that the samples synthesised in the presence of high chitosan concentration are less hydrophobic as the pre-edge peak intensity increased by a

higher factor more than the reference samples (TS-1 synthesised without chitosan) after dehydration, thereby strongly suggesting that the water molecules are coordinating with tetrahedral titanium sites.

The titanium concentration, estimated using EDS technique in each samples is presented in table 2. It can be seen that the atomic composition of the samples prepared through the PD method is very consistent throughout the series compared to slight variations observed in the titanium composition of the samples prepared by the FD technique. The variation in the titanium composition of the FD samples might be due to the extended thermal treatment to which the samples were subjected.

3.1.4 Textural Properties

Figure 9 gives the adsorption isotherms and pore size distribution of the samples. The chitosan templated samples exhibit a mixture of type I/II isotherms indicating the presence of micropores and mesopores which extend into the macropore region. This is affirmed by the pore size distribution (see fig. 9) calculated from the desorption branch of the isotherms using the density function theory (DFT) model. All the samples display a type H-3 hysteresis loop, which is typical of non-rigid aggregated plate-like particles, which are characterised by a randomly distributed slit-like pore geometry that may consist of macropore [54]. The predominantly microporous nature of the reference sample prepared through the FD method can be seen from its isotherm as it shows minimal hysteresis in the high relative pressure range and as confirmed by the pore size distribution, possess no mesopore. This implies that the mesopores in the templated samples arise from the chitosan template rather than the synthesis technique.

All the samples prepared from the PD method – including the sample prepared without chitosan – display hysteresis loop, which implies that the PD technique plays some role in the creation of extra-pores on the samples. However, there is a marked difference in the pore size distribution of the samples prepared with and without chitosan using this method. The samples prepared with chitosan showed the main peak at about 300 Å while the sample prepared without chitosan has its pore below this value, which shows the overriding/directing role of the chitosan over the method in mesopore creation. The different role of the method and the chitosan in inducing extrapore on the zeolite when the PD method is used can also be seen from table 3, where the mesopore area from the samples prepared with chitosan has higher contributions to the total surface area of their respective samples compared to the sample prepared without using chitosan.

3.1.5 Catalysis

The influence of the amount of chitosan present in the synthesis gel on the catalytic activity of the zeolite prepared from both methods was studied by the catalytic epoxidation of cyclohexene. As shown in figure 10, the conversion of cyclohexene increased with the amount of chitosan used during the catalyst preparation, which implies that pores that are larger than the intrinsic micropore of the original TS-1, which may be enhancing the accessibility of the substrate to the active sites have been successfully incorporated. The incorporation of mesoporosity and possibly macropores in the catalysts is supported by the adsorption isotherms and pore distribution given in figure 9.

Although, the inclusion of chitosan in the zeolite synthesis precursor assisted the formation of secondary pores on the zeolite structure, culminating in increase cyclohexene conversion, analysis of the reaction products shows a reduction in the selectivity towards cyclohexene epoxide. The products distribution follows the same pattern for the catalysts prepared from both the FD and PD techniques. Namely, the cyclohexene selectivity decreases with the amount of chitosan in the catalyst synthesis precursor. The decreased epoxide selectivity was accompanied by an increase in selectivity of cyclohexane diol, which is a product of hydrolysis of cyclohexene epoxide. TS-1 is typically hydrophobic, which makes it ideal in an aqueous medium of hydrogen peroxide [55], but the application of chitosan in the synthesis procedures seems to have reduced this hydrophobicity, hence, the increase in the diol selectivity. However, it is clear from both figure 11 and 12 that the catalysts prepared through the PD technique show less loss of epoxide, which implies that the loss of hydrophobicity might have originated primarily from the adopted synthesis procedure rather than the presence of chitosan in the precursor, which in turn may be attributed to the amount of water present in the synthesis precursor in both methods.

Typically, the epoxidation of cyclohexene could proceed via three different pathways, which include the catalytic transformation of the cyclohexene to the epoxide, the secondary hydration of the epoxide to diol and the non-catalytic/radical oxidation to 2-cyclohexen-1-one and 2-cyclohexen-1-ol[56-58]. Although, both 2-cyclohexen-1-one and 2-cyclohexen-1-ol were detected during this study, the amount of 2-cyclohexen-1-ol formed was well below the quantifiable level while the 2-cyclohexen-1-one formed over each catalyst is as report in figures 11 and 12.

4 Conclusions

The potential application of chitosan as a cost effective non-toxic alternative to carbon black and other carbon-based materials in the synthesis of hierarchical zeolites was successfully demonstrated. Titanium K-edge XANES analysis revealed that the titanium atoms in the TS-1 mainly exist in the tetrahedral state. The PD technique appears to enhance the incorporation of titanium in the framework compared to the FD technique. The catalytic activity of the synthesized samples was demonstrated in the epoxidation of cyclohexene using H_2O_2 as the oxidant. Whilst higher conversion of cyclohexene was achieved over chitosan templated zeolites compared to the parent samples, the selectivity towards epoxide was significantly affected. The reduced selectivity to the epoxide product was attributed to the presence of extra-framework titanium species and the reduce hydrophobicity of the samples, both of which were a consequence of the adopted synthesis technique rather than the influence of chitosan.

Acknowledgement

A. Adedigba thanks the Islamic development bank for financial award under the IDB merit scholarship program and UCL for hosting his fellowship. We also thank SSLS (Singapore) for the provision of beam time and other facilities.

References

[1] B. Notari, Microporous crystalline titanium silicates, in: D.D. Eley, W.O. Haag, B. Gates (Eds.) Advances in Catalysis, Vol 411996, pp. 253-334.

[2] P. Ratnasamy, D. Srinivas, H. Knozinger, Active sites and reactive intermediates in titanium silicate molecular sieves, in: B.C. Gates, H. Knozinger (Eds.) Advances in Catalysis, Vol 482004, pp. 1-169.

[3] P. Wu, T. Tatsumi, A new generation of titanosilicate catalyst: preparation and application to liquid-phase epoxidation of alkenes, Catalysis Surveys from Asia, 8 (2004) 137-148.

[4] W.H. Zhang, M. Froba, J.L. Wang, P.T. Tanev, J. Wong, T.J. Pinnavaia, Mesoporous titanosilicate molecular sieves prepared at ambient temperature by electrostatic (S^+I^-, $S^+X^-I^+$) and neutral (S° I°) and neutral (S° I°) assembly pathways: A comparison of physical properties and catalytic activity for peroxide oxidations, Journal of the American Chemical Society, 118 (1996) 9164-9171.

[5] A. Bhaumik, T. Tatsumi, Organically modified titanium-rich Ti-MCM-41, efficient catalysts for epoxidation reactions, Journal of Catalysis, 189 (2000) 31-39.

[6] D. He, C. Bai, C. Jiang, T. Zhou, Synthesis of titanium containing MCM-41 and its application for catalytic hydrolysis of cellulose, Powder Technology, 249 (2013) 151-156.

[7] W. Zhan, J. Yao, Z. Xiao, Y. Guo, Y. Wang, Y. Guo, G. Lu, Catalytic performance of Ti-SBA-15 prepared by chemical vapor deposition for propylene epoxidation: The effects of SBA-15 support and silylation, Microporous and Mesoporous Materials, 183 (2014) 150-155.

[8] Y. Cheneviere, F. Chieux, V. Caps, A. Tuel, Synthesis and catalytic properties of TS-1 with mesoporous/microporous hierarchical structures obtained in the presence of amphiphilic organosilanes, Journal of Catalysis, 269 (2010) 161-168.

[9] Z. Kang, G. Fang, Q. Ke, J. Hu, T. Tang, Superior Catalytic Performance of Mesoporous Zeolite TS-1 for the Oxidation of Bulky Organic Sulfides, Chemcatchem, 5 (2013) 2191-2194.

[10] X. Ke, L. Xu, C. Zeng, L. Zhang, N. Xu, Synthesis of mesoporous TS-1 by hydrothermal and steam-assisted dry gel conversion techniques with the aid of triethanolamine, Microporous and Mesoporous Materials, 106 (2007) 68-75.

[11] C.-G. Li, Y. Lu, H. Wu, P. Wu, M. He, A hierarchically core/shell-structured titanosilicate with multiple mesopore systems for highly efficient epoxidation of alkenes, Chemical Communications, 51 (2015) 14905-14908.

[12] X. Wang, G. Li, W. Wang, C. Jin, Y. Chen, Synthesis, characterization and catalytic performance of hierarchical TS-1 with carbon template from sucrose carbonization, Microporous and Mesoporous Materials, 142 (2011) 494-502.

[13] S. van Donk, A.H. Janssen, J.H. Bitter, K.P. de Jong, Generation, Characterization, and Impact of Mesopores in Zeolite Catalysts, Catalysis Reviews, 45 (2003) 297-319.

[14] C.J.H. Jacobsen, C. Madsen, J. Houzvicka, I. Schmidt, A. Carlsson, Mesoporous zeolite single crystals, Journal of the American Chemical Society, 122 (2000) 7116-7117.

[15] I. Schmidt, A. Krogh, K. Wienberg, A. Carlsson, M. Brorson, C.J.H. Jacobsen, Catalytic epoxidation of alkenes with hydrogen peroxide over first mesoporous titanium-containing zeolite, Chemical Communications, (2000) 2157-2158.

[16] A. Boisen, I. Schmidt, A. Carlsson, S. Dahl, M. Brorson, C.J.H. Jacobsen, TEM stereo-imaging of mesoporous zeolite single crystals, Chemical Communications, (2003) 958-959.

[17] A.H. Janssen, I. Schmidt, C.J.H. Jacobsen, A.J. Koster, K.P. de Jong, Exploratory study of mesopore templating with carbon during zeolite synthesis, Microporous and Mesoporous Materials, 65 (2003) 59-75.

[18] F. Schmidt, S. Paasch, E. Brunner, S. Kaskel, Carbon templated SAPO-34 with improved adsorption kinetics and catalytic performance in the MTO-reaction, Microporous and Mesoporous Materials, 164 (2012) 214-221.

[19] I. Schmidt, A. Boisen, E. Gustavsson, K. Stahl, S. Pehrson, S. Dahl, A. Carlsson, C.J.H. Jacobsen, Carbon nanotube templated growth of mesoporous zeolite single crystals, Chemistry of Materials, 13 (2001) 4416 - 4418.

[20] D. Sahu, G.M. Kannan, R. Vijayaraghavan, Carbon black particle exhibits size dependent toxicity in human monocytes, International journal of inflammation, 2014 (2014) 827019

[21] S.W. Fang, C.F. Li, D.Y.C. Shih, Antifungal activity of chitosan and its preservative effect on low-sugar candied kumquat, Journal of Food Protection, 57 (1994) 136-140.

[22] A.M. Papineau, D.G. Hoover, D. Knorr, D.F. Farkas, Antimicrobial effect of water-soluble chitosans with high hydrostatic-pressure, Food Biotechnology, Food Biotechnology, 5 (1991) 45-57.

[23] J. Berger, M. Reist, J.M. Mayer, O. Felt, N.A. Peppas, R. Gurny, Structure and interactions in covalently and ionically crosslinked chitosan hydrogels for biomedical applications, European Journal of Pharmaceutics and Biopharmaceutics, 57 (2004) 19-34.

[24] M. Kumar, A review of chitin and chitosan applications, Reactive & Functional Polymers, 46 (2000) 1-27.

[25] K. Kurita, M. Kamiya, S.I. Nishimura, Solubilization of a rigid polysaccharide - controlled partial n-acetylation of chitosan to develop solubility, Carbohydrate Polymers, 16 (1991) 83-92.

[26] J.A. Rippon, Improving the dye coverage of immature cotton fibers by treatment with chitosan, Journal of the Society of Dyers and Colourists, 100 (1984) 298-303.

[27] R.B.N. Baig, R.S. Varma, Copper on chitosan: a recyclable heterogeneous catalyst for azide-alkyne cycloaddition reactions in water, Green Chemistry, 15 (2013) 1839-1843.

[28] S.R. Hall, A.M. Collins, N.J. Wood, W. Ogasawara, M. Morad, P.J. Miedziak, M. Sankar, D.W. Knight, G.J. Hutchings, Biotemplated synthesis of catalytic Au-Pd nanoparticles, Rsc Advances, 2 (2012) 2217-2220.

[29] Y. Qin, W. Zhao, L. Yang, X. Zhang, Y. Cui, Chitosan-Based Heterogeneous Catalysts for Enantioselective Michael Reaction, Chirality, 24 (2012) 640-645.

[30] M. Zeng, C. Qi, X.-m. Zhang, Chitosan microspheres supported palladium heterogeneous catalysts modified with pearl shell powders, International Journal of Biological Macromolecules, 55 (2013) 240-245.

[31] X. Chen, H. Yang, Z.Y. Gu, Z.Z. Shao, Preparation and characterization of HY zeolite-filled chitosan membranes for pervaporation separation, Journal of Applied Polymer Science, 79 (2001) 1144-1149.

[32] W.S.W. Ngah, L.C. Teong, M.A.K.M. Hanafiah, Adsorption of dyes and heavy metal ions by chitosan composites: A review, Carbohydrate Polymers, 83 (2011) 1446-1456.

[33] Y. Du, Y. Zhu, S. Xi, P. Yang, H.O. Moser, M.B.H. Breese, A. Borgna, XAFCA: a new XAFS beamline for catalysis research, Journal of Synchrotron Radiation, 22 (2015) 839-843.

[34] G. Sankar, J.M. Thomas, C.R.A. Catlow, C.M. Barker, D. Gleeson, N. Kaltsoyannis, The three-dimensional structure of the titanium-centered active site during steady-state catalytic epoxidation of alkenes, Journal of Physical Chemistry B, 105 (2001) 9028-9030.

[35] R. Giudici, H.W. Kouwenhoven, R. Prins, Comparison of nitric and oxalic acid in the dealumination of mordenite, Applied Catalysis A-General, 203 (2000) 101-110.

[36] J.-B. Koo, N. Jiang, S. Saravanamurugan, M. Bejblova, Z. Musilova, J. Cejka, S.-E. Park, Direct synthesis of carbon-templating mesoporous ZSM-5 using microwave heating, Journal of Catalysis, 276 (2010) 327-334.

[37] X. Li, R. Prins, J.A. van Bokhoven, Synthesis and characterization of mesoporous mordenite, Journal of Catalysis, 262 (2009) 257-265.

[38] M. Ogura, S.Y. Shinomiya, J. Tateno, Y. Nara, E. Kikuchi, H. Matsukata, Formation of uniform mesopores in ZSM-5 zeolite through treatment in alkaline solution, Chemistry Letters, (2000) 882-883.

[39] M. Ogura, S.Y. Shinomiya, J. Tateno, Y. Nara, M. Nomura, E. Kikuchi, M. Matsukata, Alkali-treatment technique - New method for modification of structural and acid-catalytic properties of ZSM-5 zeolites, Applied Catalysis A-General, 219 (2001) 33-43.

[40] C. Madsen, C.J.H. Jacobsen, Nanosized zeolite crystals - convenient control of crystal size distribution by confined space synthesis, Chemical Communications, (1999) 673-674.

[41] I. Schmidt, C. Madsen, C.J.H. Jacobsen, Confined space synthesis. A novel route to nanosized zeolites, Inorganic Chemistry, 39 (2000) 2279-2283.

[42] J. Dai, W. Zhong, W. Yi, M. Liu, L. Mao, Q. Xu, D. Yin, Bifunctional H2WO4/TS-1 catalysts for direct conversion of cyclohexane to adipic acid: Active sites and reaction steps, Applied Catalysis B: Environmental, 192 (2016) 325-341.

[43] S. Bordiga, A. Damin, F. Bonino, G. Ricchiardi, A. Zecchina, R. Tagliapietra, C. Lamberti, Resonance Raman effects in TS-1: the structure of Ti(IV) species and reactivity towards H2O, NH3 and H2O2: an in situ study, Physical Chemistry Chemical Physics, 5 (2003) 4390-4393.

[44] Q. Guo, K. Sun, Z. Feng, G. Li, M. Guo, F. Fan, C. Li, A Thorough Investigation of the Active Titanium Species in TS-1 Zeolite by In Situ UV Resonance Raman Spectroscopy, Chemistry-a European Journal, 18 (2012) 13854-13860.

[45] C. Li, G. Xiong, Q. Xin, J.K. Liu, P.L. Ying, Z.C. Feng, J. Li, W.B. Yang, Y.Z. Wang, G.R. Wang, X.Y. Liu, M. Lin, X.Q. Wang, E.Z. Min, UV resonance Raman spectroscopic identification of titanium atoms in the framework of TS-1 zeolite, Angewandte Chemie-International Edition, 38 (1999) 2220-2222.

[46] F.Z. Zhang, X.W. Guo, X.S. Wang, G. Li, J.C. Zhou, J.Q. Yu, C. Li, The active sites in different TS-1 zeolites for propylene epoxidation studied by ultraviolet resonance Raman and ultraviolet visible absorption spectroscopies, Catalysis Letters, 72 (2001) 235-239.

[47] B.F.G. Johnson, M.C. Klunduk, C.M. Martin, G. Sankar, S.J. Teate, J.M. Thomas, The preparation, molecular structure and catalytic relevance of Ti(OSiPh(3))(4) and Ti(OGePh(3))(4), Journal of Organometallic Chemistry, 596 (2000) 221-225.

[48] J.M. Thomas, G. Sankar, The role of XAFS in the in situ and ex situ elucidation of active sites in designed solid catalysts, Journal of Synchrotron Radiation, 8 (2001) 55-60.

[49] C.M. Barker, D. Gleeson, N. Kaltsoyannis, C.R.A. Catlow, G. Sankar, J.M. Thomas, On the structure and coordination of the oxygen-donating species in Ti up arrow MCM-41/TBHP oxidation catalysts: a density functional theory and EXAFS study, Physical Chemistry Chemical Physics, 4 (2002) 1228-1240.

[50] S. Bordiga, F. Bonino, A. Damin, C. Lamberti, Reactivity of Ti(IV) species hosted in TS-1 towards H2O2-H2O Solutions investigated by ab initio cluster and periodic approaches combined with experimental XANES and EXAFS data: a review and new highlights, Physical Chemistry Chemical Physics, 9 (2007) 4854-4878.

[51] E. Gianotti, V. Dellarocca, M.L. Pena, F. Rey, A. Corma, S. Coluccia, L. Marchese, Unequivocal evidence of the presence of titanols in Ti-MCM-48 mesoporous materials. A combined diffuse reflectance UV-Vis-Nir and Si-29-MAS-NMR study, Research on Chemical Intermediates, 30 (2004) 871-877.

[52] L. Marchese, E. Gianotti, V. Dellarocca, T. Maschmeyer, F. Rey, S. Coluccia, J.M. Thomas, Structure-functionality relationships of grafted Ti-MCM41 silicas. Spectroscopic and catalytic studies, Physical Chemistry Chemical Physics, 1 (1999) 585-592.

[53] D. Srinivas, P. Manikandan, S.C. Laha, R. Kumar, P. Ratnasamy, Reactive oxo-titanium species in titanosilicate molecular sieves: EPR investigations and structure-activity correlations, Journal of Catalysis, 217 (2003) 160-171.

[54] M. Thommes, K. Kaneko, V. Neimark Alexander, P. Olivier James, F. Rodriguez-Reinoso, J. Rouquerol, S.W. Sing Kenneth, Physisorption of gases, with special reference to the evaluation

of surface area and pore size distribution (IUPAC Technical Report), Pure and Applied Chemistry2015, pp. 1051.

[55] C.B. Khouw, C.B. Dartt, J.A. Labinger, M.E. Davis, Studies on the catalytic-oxidation of alkanes and alkenes by titanium silicates, Journal of Catalysis, 149 (1994) 195-205.

[56] Y. Cao, H. Yu, F. Peng, H. Wang, Selective Allylic Oxidation of Cyclohexene Catalyzed by Nitrogen-Doped Carbon Nanotubes, ACS Catalysis, 4 (2014) 1617-1625.

[57] J. Vernimmen, M. Guidotti, J. Silvestre-Albero, E.O. Jardim, M. Mertens, O.I. Lebedev, G. Van Tendeloo, R. Psaro, F. Rodríguez-Reinoso, V. Meynen, P. Cool, Immersion calorimetry as a tool to evaluate the catalytic performance of titanosilicate materials in the epoxidation of cyclohexene, Langmuir, 27 (2011) 3618-3625.

[58] J. Wang, L. Xu, K. Zhang, H. Peng, H. Wu, J.-g. Jiang, Y. Liu, P. Wu, Multilayer structured MFI-type titanosilicate: Synthesis and catalytic properties in selective epoxidation of bulky molecules, Journal of Catalysis, 288 (2012) 16-23.

Tables

Table 1 – Comparison of the Pre-edge peak intensities of the samples obtained from in situ Ti Kedge XANES for the samples prepared through the FD and PD techniques

	Pre-edge intensity			
	FD		PD	
	Hydrated	Dehydrated	Hydrated	Dehydrated
TS-1 with 0% chitosan	0.53	0.57	0.56	0.6
TS-1 with 5% chitosan	0.48	0.6	0.52	0.57
TS-1 with 10% chitosan	0.40	0.44	0.50	0.59
Model compound $Ti(OSiPh_3)_4$	0.69			
Model compound ETS-10	0.14			

Table 2 – Atomic titanium composition of samples measured by EDS

	$\left(\frac{Ti}{Si+Ti}\right)$	
	FD	PD
TS-1 with 0% chitosan	0.021	0.026
TS-1 with 5% chitosan	0.018	0.027
TS-1 with 10% chitosan	0.025	0.025

Table 3: Textural properties of samples prepared from FD and PD methods

Samples	Total surface area (m^2/g)	Micropore area (m^2/g)	Mesopore area (m^2/g)
FD samples			
TS-1 with 0% chitosan	411	365	46
TS-1 with 5% chitosan	504	443	61
TS-1 with 10% chitosan	474	406	68
PD samples			
TS-1 with 0% chitosan	490	431	59
TS-1 with 5% chitosan	405	327	78
TS-1 with10% chitosan	347	271	76

Figure captions

Figure 1 – XRD patterns of TS-1 samples prepared without and with two different concentrations of chitosan using the (a) FD and (b) PD techniques

Figure 2 – SEM Micrograph of TS-1 samples prepared in the absence and presence of two different chitosan concentrations. The left panel shows samples prepared using the FD method and the right panel are samples prepared via the PD method.

Figure 3 – FTIR spectra of the TS-1 samples prepared using FD (top) and PD (bottom) techniques. Note that only a narrow region between 400 and 1200 cm^{-1} is shown for clarity. The characteristic band due to the Ti^{4+} substitution at 960 cm^{-1} is arrowed.

Figure 4 – Typical Raman Spectra of the three different TS-1 synthesized using Chitosan as a secondary template. The 960 cm^{-1} and 1125 cm^{-1} band are arrowed. (a) Samples prepared through FD precursors and (b) using PD precursors

Figure 5 – Ti K-edge XAS of Chitosan templated TS-1 compared with two model compounds of with known titanium coordination. (a) Samples from the FD method (b) samples from PD method. Please note that the spectra are offset in the vertical direction.

Figure 6 – UV-vis spectra of samples from FD (top) and PD (bottom) methods showing the presence of extra-framework titanium in the FD samples

Figure 7 – *In situ* XAS spectra of samples synthesized through the FD method with (a) 0% (b) 5% and (c) 10% chitosan in the starting precursor. The spectra show an increase

in the pre-edge intensity as the samples were dehydrated in a vacuum at 750 K. inset is an expanded pre-edge region for clarity.

Figure 8 – *In situ* XAS spectra of samples synthesized through the PD method with (a) 0% (b) 5% and (c) 10% chitosan in the starting precursor. The spectra show an increase in the pre-edge intensity as the samples were dehydrated in vacuum at 750 K. Inset is an expanded pre-edge region for clarity

Figure 9 – Adsorption Isotherm (top) and pore size distribution (bottom) of all the samples synthesised with and without chitosan. Samples prepared from the FD precursor are in the left column and PD precursor is in the right column

Figure 10 – Effect of the amount of chitosan in the synthesis precursor on the catalytic conversion of cyclohexene. Reaction conditions: temperature; 333K, reaction time; 6 hours, cyclohexene : H_2O_2; 1:1

Figure 11 – Effect of the amount of chitosan in the synthesis precursor on product selectivity for samples prepared through the FD methods

Figure 12 – Effect of the amount of chitosan in the synthesis precursor on product selectivity for samples prepared through the PD methods

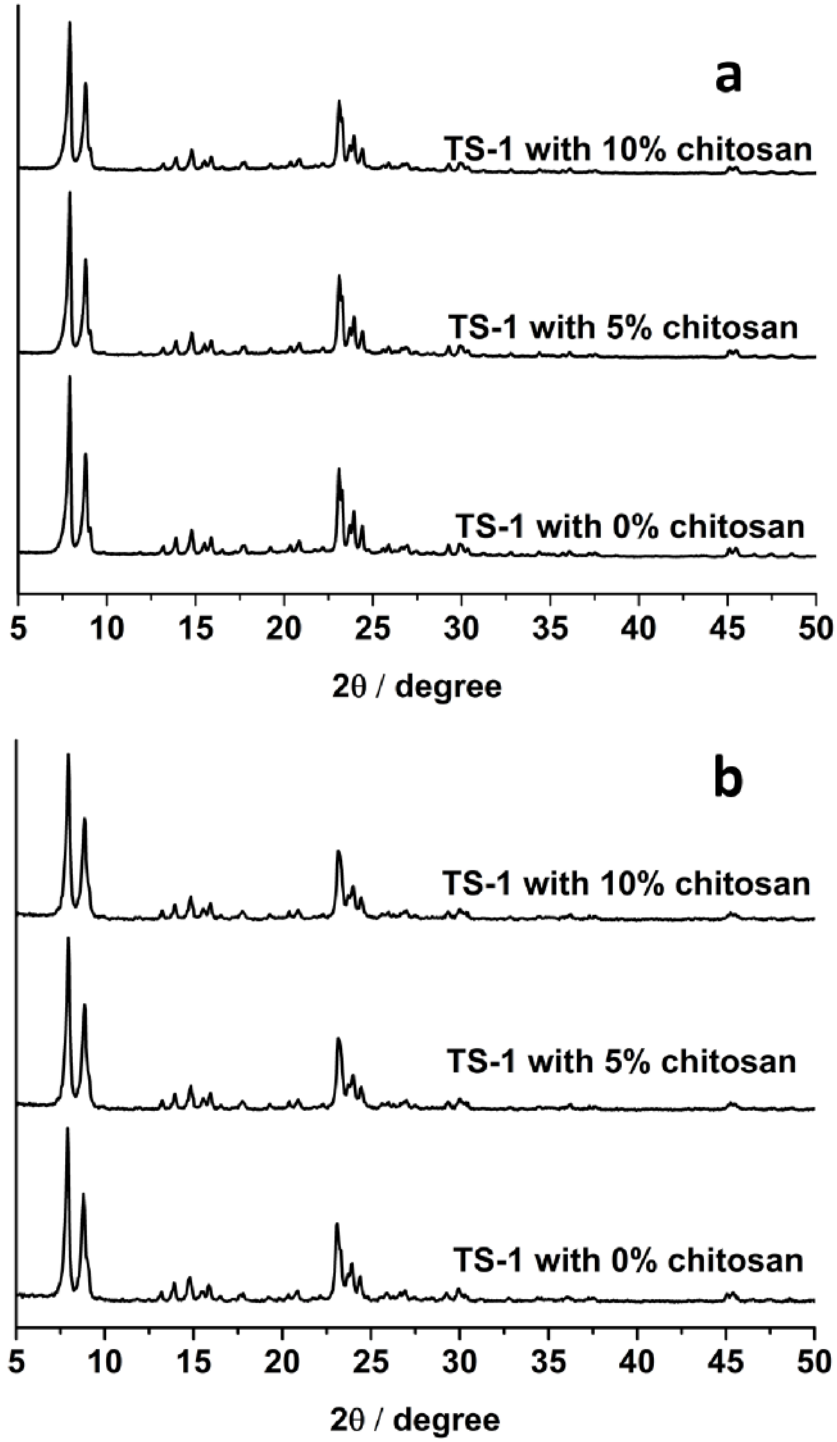
a
TS-1 with 10% chitosan
TS-1 with 5% chitosan
TS-1 with 0% chitosan
5 10 15 20 25 30 35 40 45 50
2θ / degree
b
TS-1 with 10% chitosan
TS-1 with 5% chitosan
TS-1 with 0% chitosan
5 10 15 20 25 30 35 40 45 50
2θ / degree

Figure 1

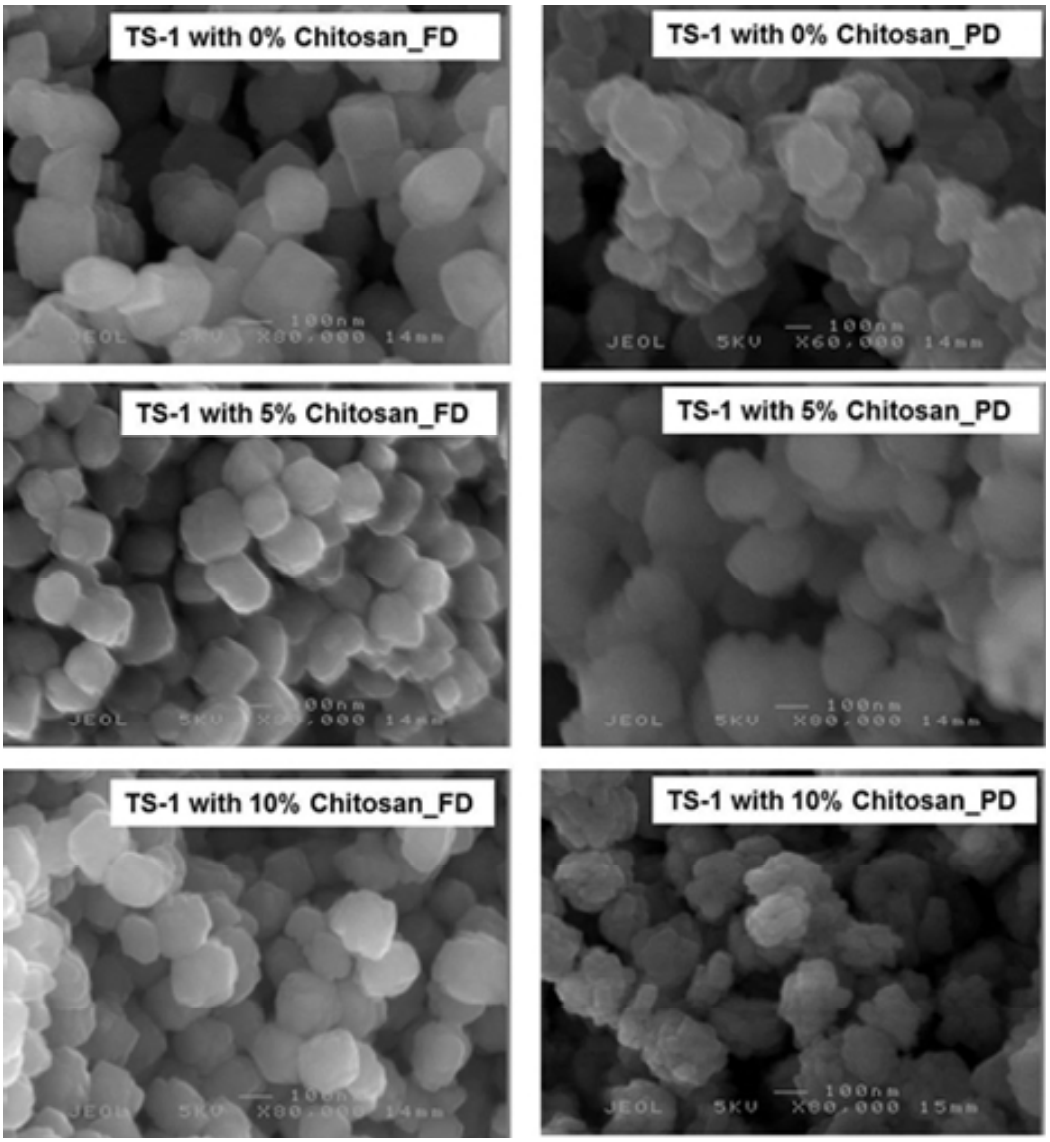
TS-1 with 0% Chitosan_FD
TS-1 with 0% Chitosan_PD
TS-1 with 5% Chitosan_FD
TS-1 with 5% Chitosan_PD
TS-1 with 10% Chitosan_FD
TS-1 with 10% Chitosan_PD

Figure 2

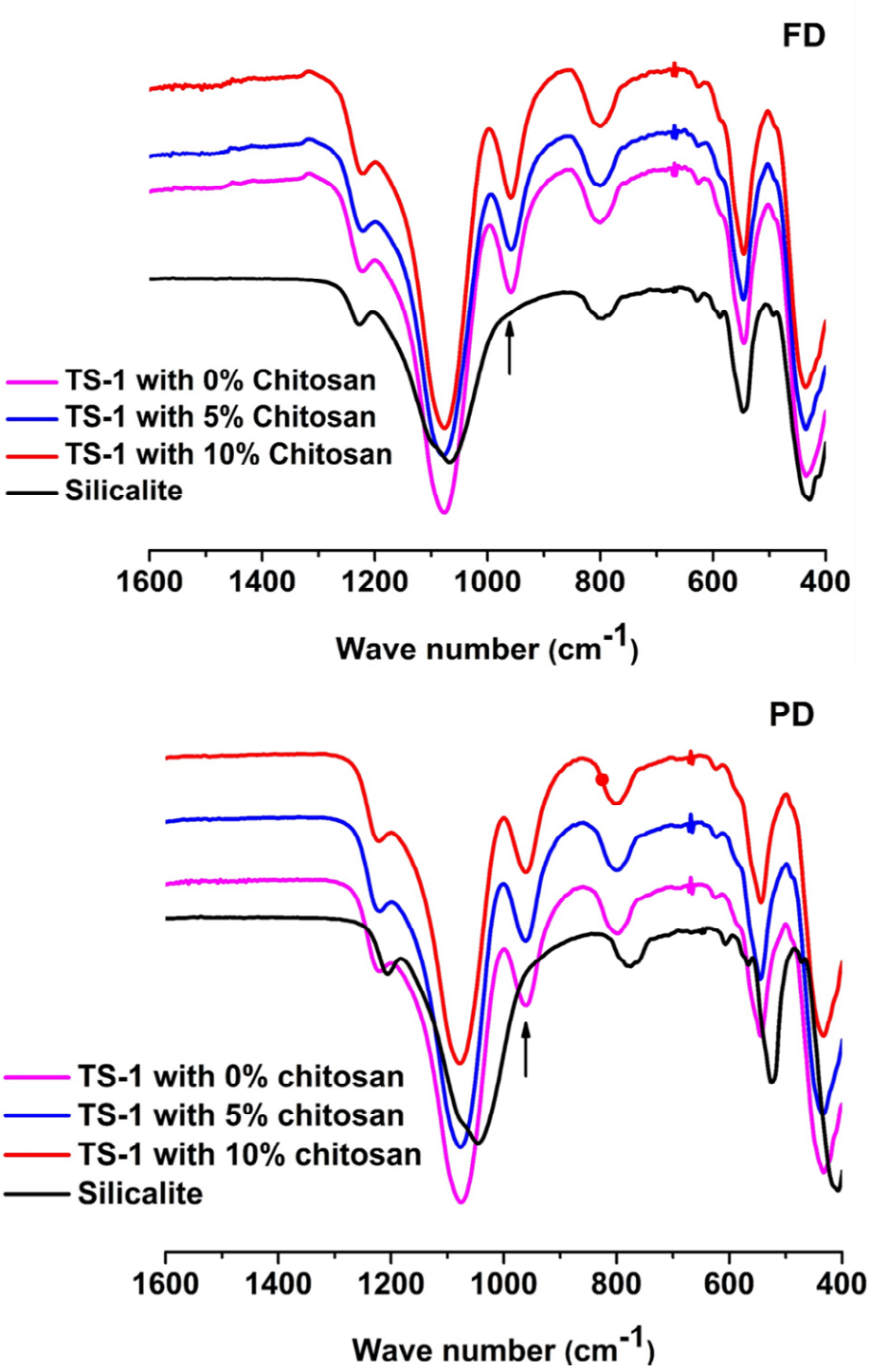
FD
TS-1 with 0% Chitosan
TS-1 with 5% Chitosan
TS-1 with 10% Chitosan
Silicalite
1600
1400
1200
1000
800
600
400
Wave number (cm-1)
PD
TS-1 with 0% chitosan
TS-1 with 5% chitosan
TS-1 with 10% chitosan
Silicalite
1600
1400
1200
1000
800
600
400
Wave number (cm-1)

Figure 3

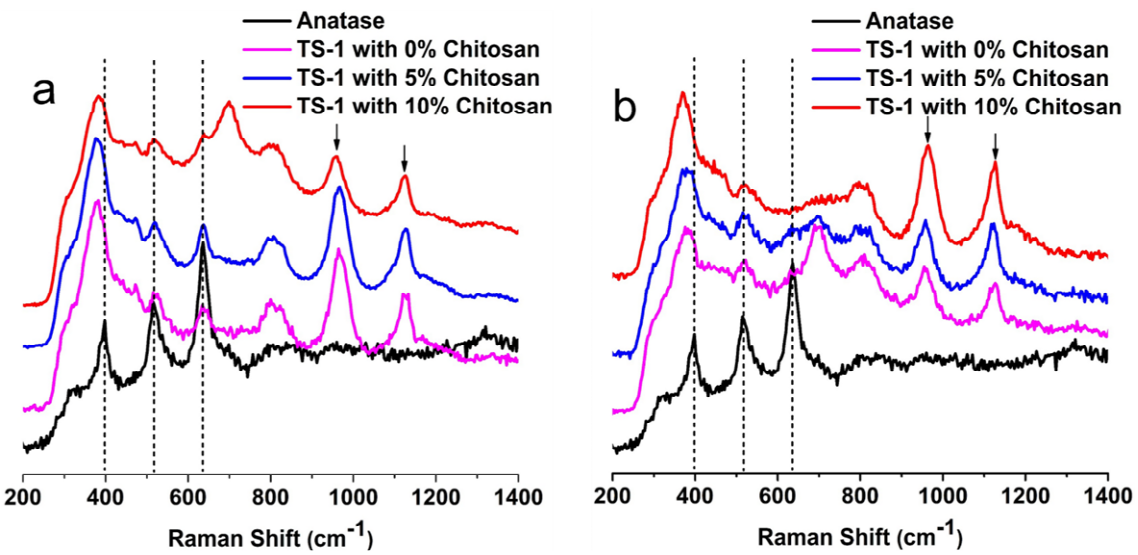
a
Anatase
TS-1 with 0% Chitosan
TS-1 with 5% Chitosan
TS-1 with 10% Chitosan
200
400
600
800
1000
1200
1400
Raman Shift (cm-1)
b
Anatase
TS-1 with 0% Chitosan
TS-1 with 5% Chitosan
TS-1 with 10% Chitosan
200
400
600
800
1000
1200
1400
Raman Shift (cm-1)

Figure 4

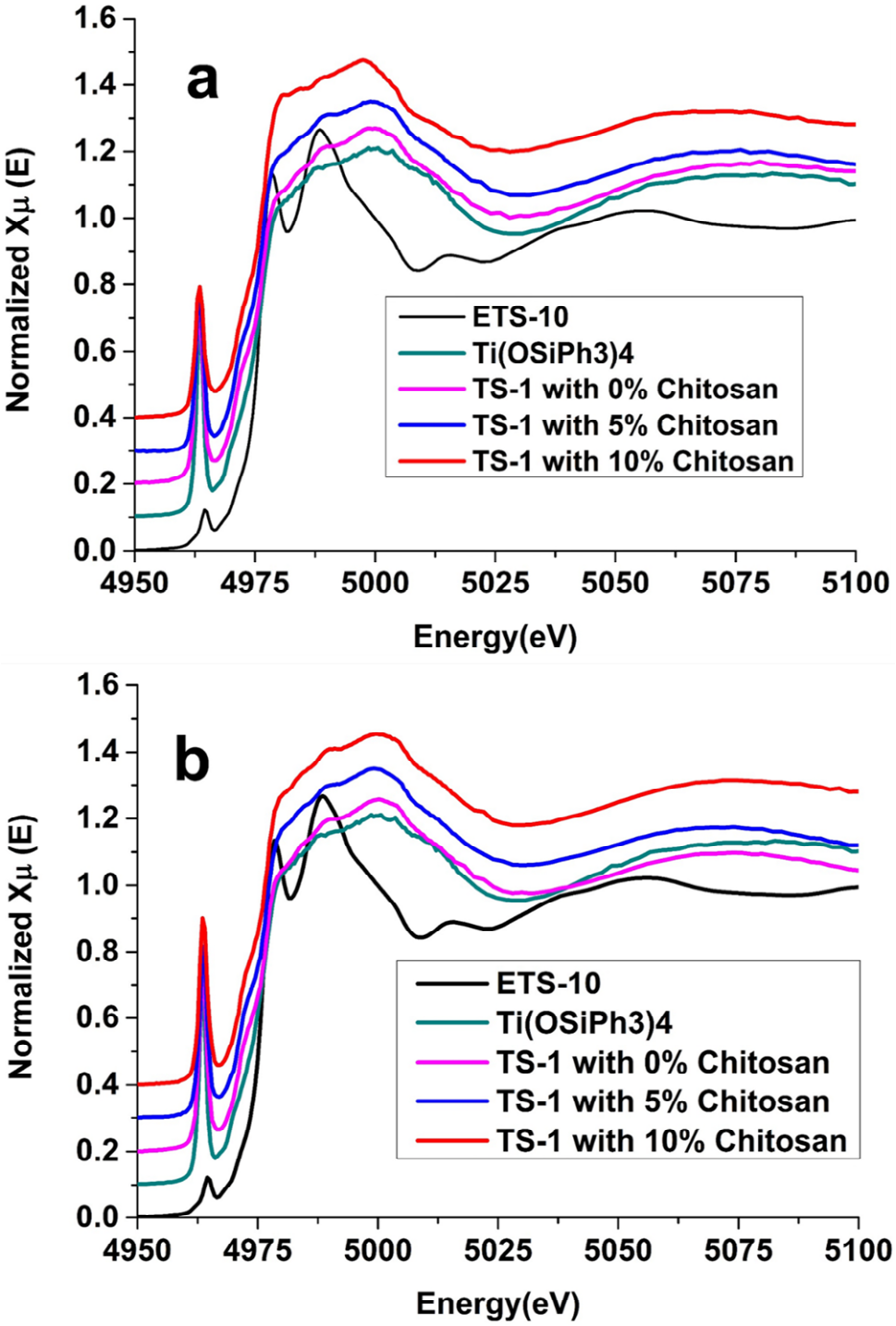
a
b
Normalized Xμ (E)
Energy(eV)
ETS-10
Ti(OSiPh3)4
TS-1 with 0% Chitosan
TS-1 with 5% Chitosan
TS-1 with 10% Chitosan
0.0
0.2
0.4
0.6
0.8
1.0
1.2
1.4
1.6
4950
4975
5000
5025
5050
5075
5100

Figure 5

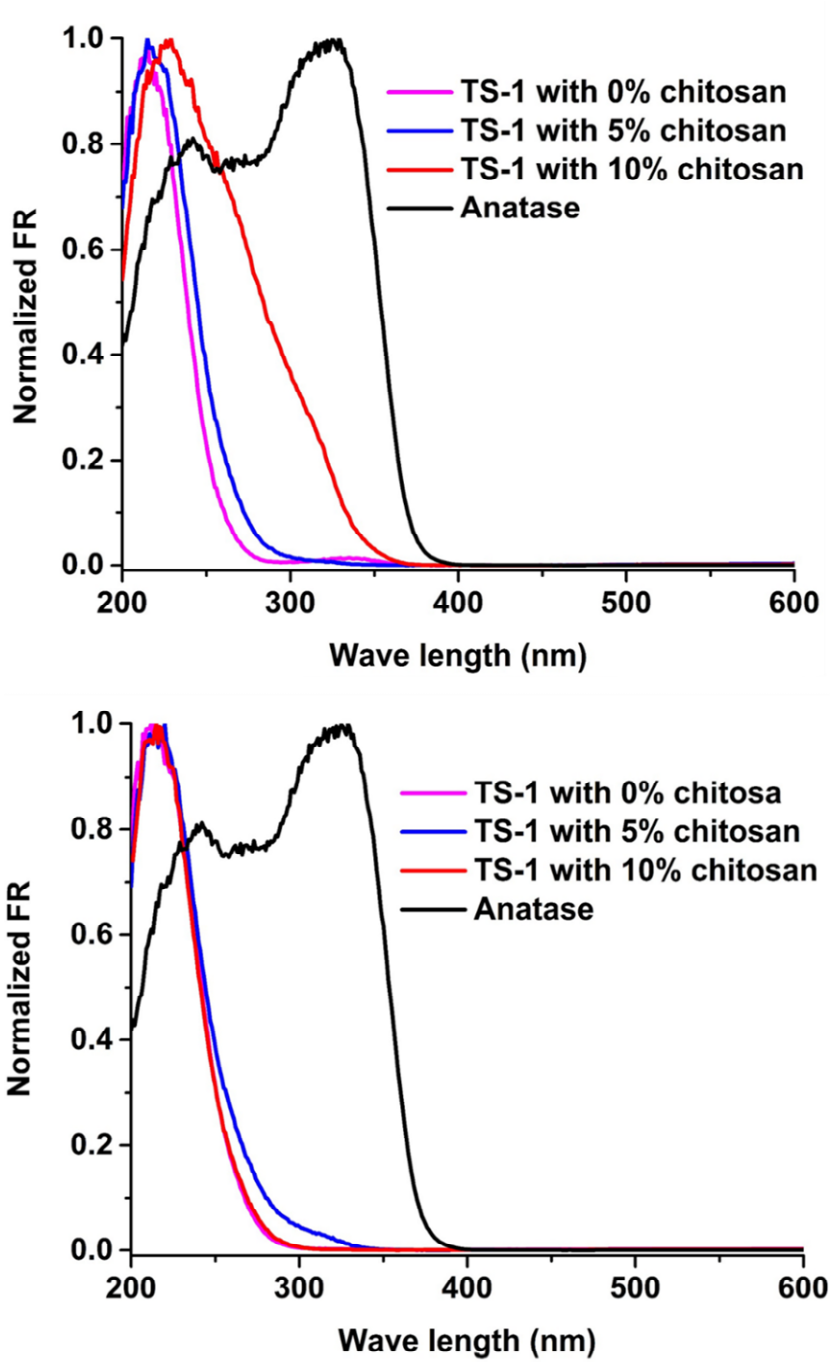
1.0
0.8
0.6
0.4
0.2
0.0
Normalized FR
200
300
400
500
600
Wave length (nm)
TS-1 with 0% chitosan
TS-1 with 5% chitosan
TS-1 with 10% chitosan
Anatase
1.0
0.8
0.6
0.4
0.2
0.0
Normalized FR
200
300
400
500
600
Wave length (nm)
TS-1 with 0% chitosa
TS-1 with 5% chitosan
TS-1 with 10% chitosan
Anatase

Figure 6

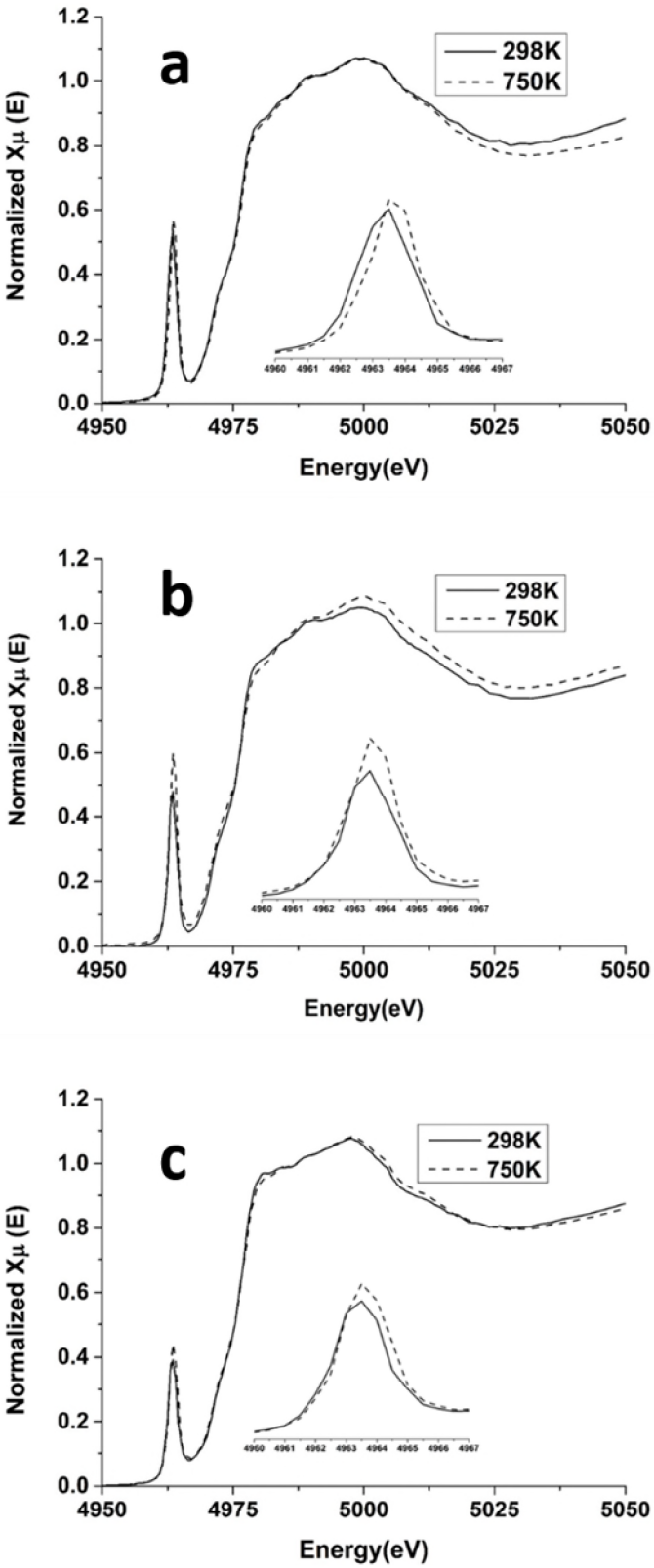
a
298K
750K
Normalized Xμ (E)
Energy(eV)
b
298K
750K
Normalized Xμ (E)
Energy(eV)
c
298K
750K
Normalized Xμ (E)
Energy(eV)

Figure 7

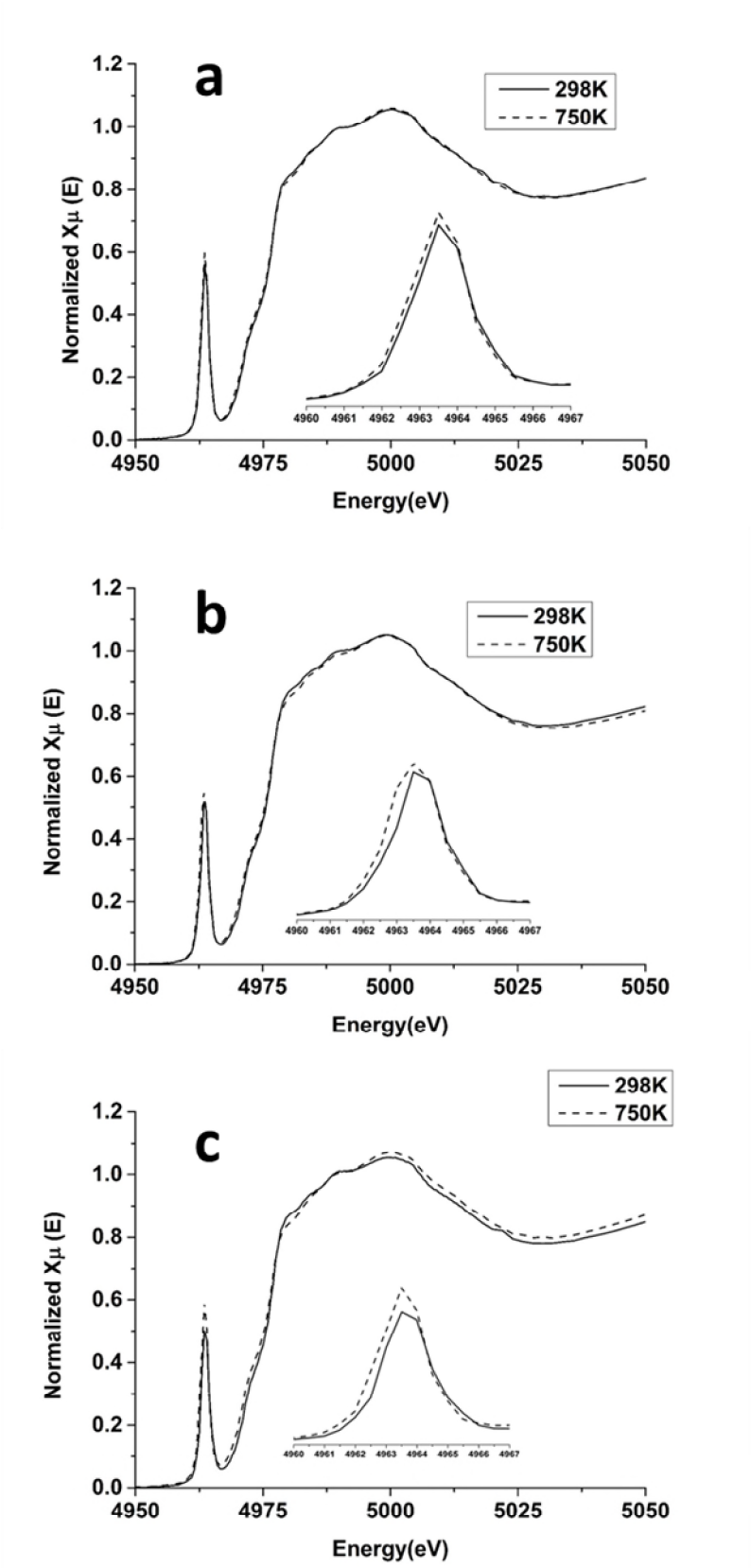
a
298K
750K
Normalized Xμ (E)
Energy(eV)
b
298K
750K
Normalized Xμ (E)
Energy(eV)
c
298K
750K
Normalized Xμ (E)
Energy(eV)

Figure 8

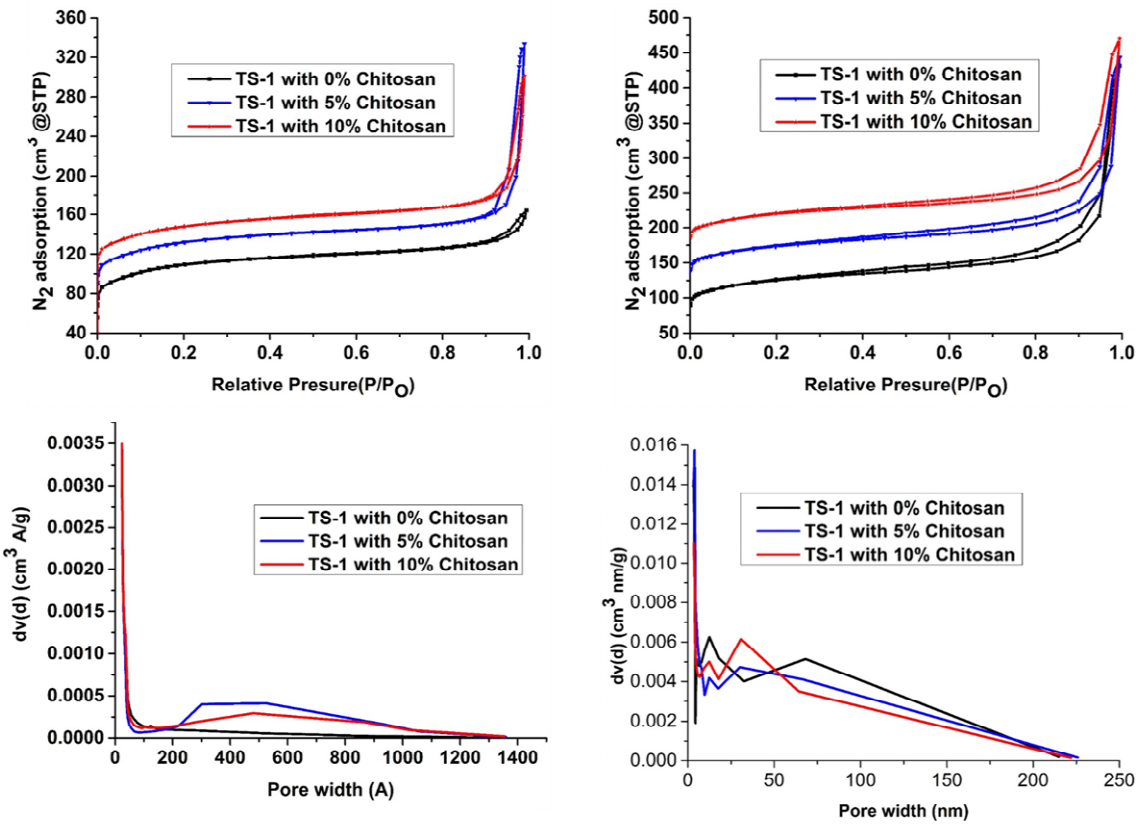
TS-1 with 0% Chitosan
TS-1 with 5% Chitosan
TS-1 with 10% Chitosan
N2 adsorption (cm3 @STP)
Relative Presure(P/PO)
dv(d) (cm3 A/g)
Pore width (A)
dv(d) (cm3 nm/g)
Pore width (nm)

Figure 9

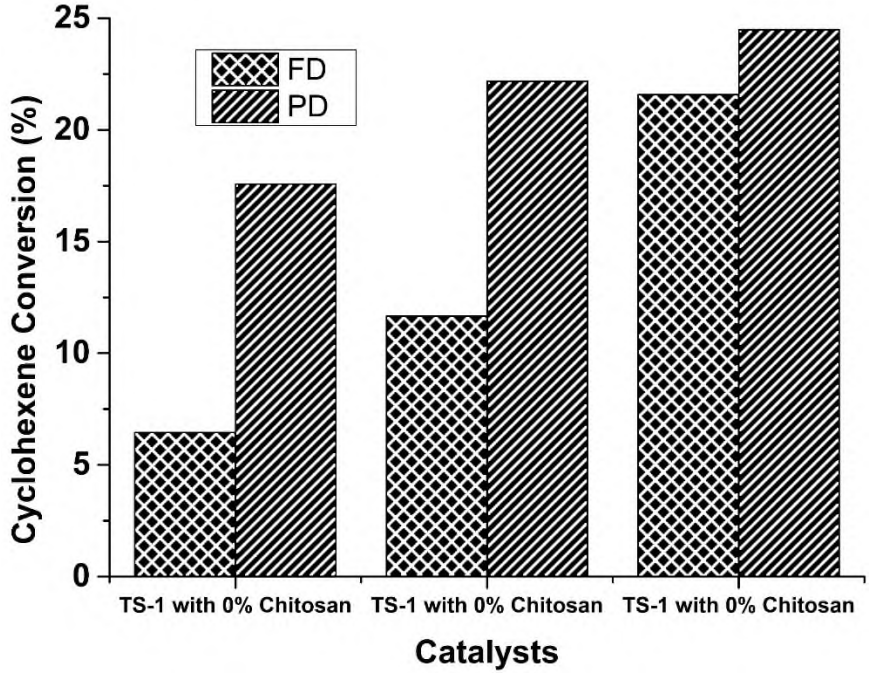

Figure 10

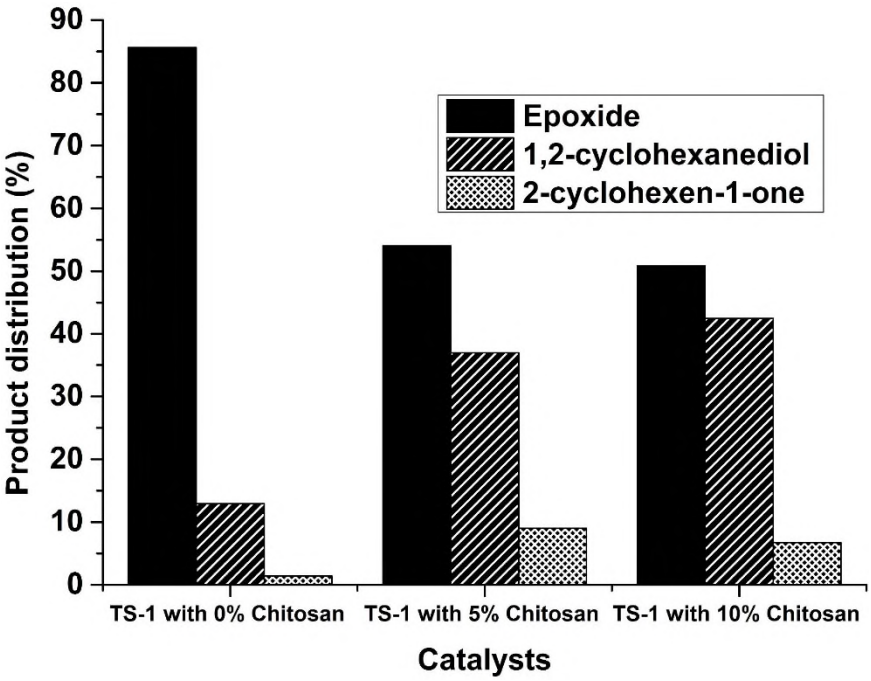

Figure 11

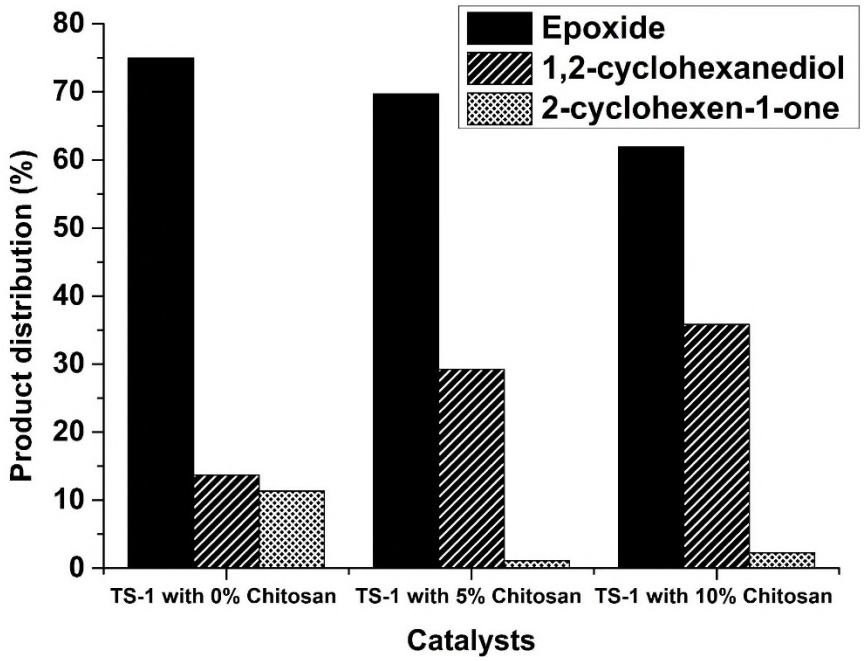
Epoxide
1,2-cyclohexanediol
2-cyclohexen-1-one
Product distribution (%)
80
70
60
50
40
30
20
10
0
TS-1 with 0% Chitosan
TS-1 with 5% Chitosan
TS-1 with 10% Chitosan
Catalysts

Figure 12